Physics Letters B 705 (2011) 65–70

Contents lists available at SciVerse ScienceDirect

Physics Letters B

www.elsevier.com/locate/physletb

Evidence for α-particle condensation in nuclei from the Hoyle state deexcitation

Ad.R. Raduta [a,b,*], B. Borderie [a], E. Geraci [c,d,e], N. Le Neindre [a,f], P. Napolitani [a], M.F. Rivet [a], R. Alba [g], F. Amorini [g], G. Cardella [c], M. Chatterjee [h], E. De Filippo [c], D. Guinet [i], P. Lautesse [i], E. La Guidara [c,j], G. Lanzalone [g,k], G. Lanzano [c,1], I. Lombardo [g,d], O. Lopez [f], C. Maiolino [g], A. Pagano [c], S. Pirrone [c], G. Politi [c,d], F. Porto [g,d], F. Rizzo [g,d], P. Russotto [g,d], J.P. Wieleczko [l]

[a] *Institut de Physique Nucléaire, CNRS/IN2P3, Université Paris-Sud 11, Orsay, France*
[b] *National Institute for Physics and Nuclear Engineering, Bucharest-Magurele, Romania*
[c] *INFN, Sezione di Catania, Italy*
[d] *Dipartimento di Fisica e Astronomia, Università di Catania, Italy*
[e] *INFN, Sezione di Bologna and Dipartimento di Fisica, Università di Bologna, Italy*
[f] *LPC, CNRS/IN2P3, Ensicaen, Université de Caen, Caen, France*
[g] *INFN, Laboratori Nazionali del Sud, Catania, Italy*
[h] *Saha Institute of Nuclear Physics, Kolkata, India*
[i] *Institut de Physique Nucléaire, CNRS/IN2P3, Université Claude Bernard Lyon 1, Villeurbanne, France*
[j] *CSFNSM, Catania, Italy*
[k] *Università di Enna "Kore", Enna, Italy*
[l] *GANIL (DSM-CEA/CNRS/IN2P3), Caen, France*

ARTICLE INFO

Article history:
Received 27 April 2011
Received in revised form 30 September 2011
Accepted 6 October 2011
Available online 8 October 2011
Editor: J.-P. Blaizot

Keywords:
Heavy ion reactions
Correlation functions
α-particle condensation
Cluster model
Nuclear structure

ABSTRACT

The fragmentation of quasi-projectiles from the nuclear reaction $^{40}Ca + {}^{12}C$ at 25 MeV/nucleon was used to produce excited states candidates to α-particle condensation. Complete kinematic characterization of individual decay events, made possible by a high-granularity 4π charged particle multi-detector, reveals that $7.5 \pm 4.0\%$ of the particle decays of the Hoyle state correspond to direct decays in three equal-energy α-particles.

Bose–Einstein condensation is known to occur in weakly and strongly interacting systems such as dilute atomic gases and liquid ^{4}He [1]. During the last decade it was theoretically shown that dilute symmetric nuclear matter may also experience Bose particle condensation [2–4]. More precisely, for densities smaller than one fifth of the nuclear saturation density, nuclear matter organizes itself in α-clusters, while for higher densities the 2-nucleon deuteron condensation is preferred. This new possible phase of nuclear matter may have its counterpart in low-density states of self conjugate lighter nuclei, in the same way as superfluid nuclei are the finite-size counterpart of superfluid nuclear and neutron matter. This means that under some circumstances, the α condensation, i.e. bosonic properties, might dominate over the nucleon properties even in finite nuclei.

Considerable advance in favor of α-particle condensation in nuclei is provided by the excellent theoretical description of the Hoyle state (i.e. the first 0^+ excited state at 7.654 MeV of ^{12}C) and of the 0^+_6 state at 15.097 MeV of ^{16}O in terms of condensate type wave functions [5,6]. The case of the Hoyle state is particularly suggestive as both shell-model and no-core shell model calculations are known to fail in describing it. Recent Fermionic Molecular Dynamics (FMD) calculations [7] plead in favor of a more nuanced interpretation of the Hoyle state structure, that is a mixture of various pre-formed α-configurations. This scenario agrees with the pioneering works of Uegaki et al. [8] where acute-angle, bent and linear chain configurations were identified. In what regards the

* Corresponding author at: National Institute for Physics and Nuclear Engineering, Bucharest-Magurele, Romania.
E-mail address: araduta@nipne.ro (Ad.R. Raduta).
[1] Deceased.

0370-2693/$ – see front matter
doi:10.1016/j.physletb.2011.10.008

expected diluteness, coupled channel analysis [9] of experimental data confirm theoretical works [5] estimating the rms radius of the Hoyle state as 45% larger than the radius of ^{12}C in its ground state. More generally, α-particle condensation is conjectured to be a generic feature of medium-size self-conjugated $4N$ nuclei whose excitation lies in the vicinity of the $N\alpha$ decay threshold [10,11].

The aim of the present Letter is to search from the experimental side a direct evidence for α-particle condensation from the Hoyle state. According to the present understanding of the Hoyle state: a gas-like structure of three α-particles which occupy dominantly the lowest S orbit, such an evidence may be judged from the simultaneous emission of three α-particles with very low kinetic energy dispersion. As it is experimentally difficult to identify and measure α-particles with low energy, probably the most appropriate strategy, chosen in this work, should involve high velocity reaction products in the laboratory (to take advantage of velocity boosts) detected by a high granularity-high solid angle particle array (to precisely reconstruct the directions of velocity vectors). The existence of the direct decay channel was firstly investigated in Ref. [12] and its contribution to the total α decay (dominated by the $^{8}\mathrm{Be}_{\mathrm{g.s.}} + \alpha$ sequential decay) was estimated to be at most 4%. The existence of such a decay channel is also of the greatest importance for nuclear astrophysics, due to the crucial role played by the Hoyle state for the synthesis of ^{12}C in the universe [13,14].

The data reported here have been obtained in the nuclear reaction $^{40}\mathrm{Ca} + {}^{12}\mathrm{C}$ at 25 MeV per nucleon incident energy performed at INFN, Laboratori Nazionali del Sud in Catania, Italy. The beam impinging on a thin carbon target (320 μg/cm^2) was delivered by the Superconducting Cyclotron and the charged reaction products were detected by the CHIMERA 4π multi-detector [15]. The beam intensity was kept around 10^7 ions/s to avoid pile-up events. CHIMERA consists of 1192 silicon-CsI(Tl) telescopes mounted on 35 rings covering 94% of the solid angle, with polar angle ranging from 1 to 176°. The solid angle corresponding to each module is not uniform, but varies between 0.13 msr at forward angles and 35.4 msr at the most backward angles. Among the most interesting characteristics of CHIMERA are the low detection and identification thresholds for light charged particles (LCP) and the very high granularity at forward angles. The mass and charge of the detected nuclei were determined by the energy–time of flight method (TOF) for LCP stopped in silicon detectors and $\Delta E - E$ ($Z > 5$) and shape identification ($Z \leqslant 5$) techniques for charged products stopped in CsI(Tl). In addition ^{8}Be nuclei (two equal-energy α's hitting the same crystal) were identified in CsI(Tl) [16]. The energy of detected nuclei was measured by the Si detectors calibrated using proton, carbon and oxygen beams at various energies ranging from 10 to 100 MeV. For $Z = 2$, dedicated energy calibrations of the fast component of CsI(Tl) light was realized using the TOF. Though high-quality TOF charts allowing for a direct calibration of the CsI light exist only for 60% of the total number of modules, we have finally managed to calibrate more than 95% of modules from 1 to 62°. The modules for which TOF information was poor or missing were calibrated by comparing the fast component distribution with the benchmark distribution of the corresponding ring built out of the telescopes with excellent TOF. The energy resolution for α-particles varies between 1.0 and 2.5% depending on the module.

Complete kinematical characterization of the reaction products allows one to identify the particle emitting sources using invariant velocity plots in the $\gamma\beta_\perp$ vs. $1/2\log[(E+p_\parallel)/(E-p_\parallel)]$ plane. E, $p_\parallel$, $p_\perp$ stand for the energy and momentum components along and, respectively, perpendicular to the beam axis, $\beta = v/c$ is the reduced velocity and $\gamma = 1/\sqrt{1-\beta^2}$. The invariant velocity plot corresponding to events having an α-multiplicity of at least 3 is depicted in Fig. 1. It shows the dominant binary character of the collisions with the formation of a quasi-projectile (QP) and a quasi-target (QT) not studied in this experiment. The QP source may be easily isolated by requiring a rapidity of reaction products larger than $y_{\mathrm{proj}}/2$, where y_{proj} is the projectile rapidity. Hereafter, we shall focus exclusively on QP decay products with $m_\alpha = 3$.

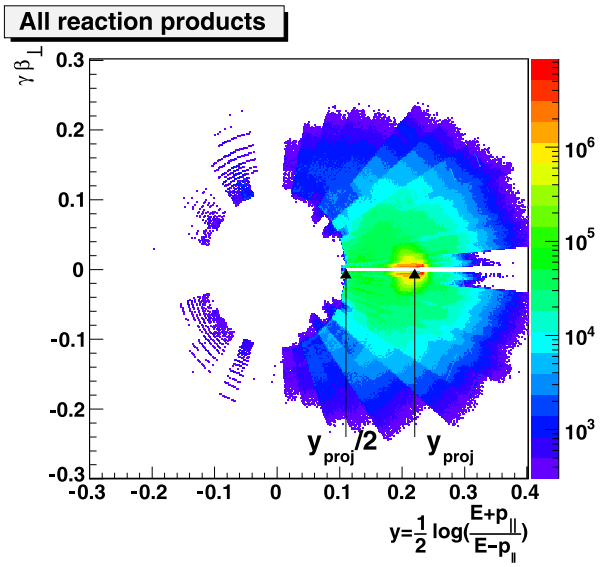

Fig. 1. (Color online.) Invariant velocity plot corresponding to all reaction products obtained in $^{40}\mathrm{Ca} + {}^{12}\mathrm{C}$ at 25 MeV/nucleon. The considered events have $m_\alpha \geqslant 3$. The vertical arrows indicate the projectile rapidity and its half.

With the aim of investigating the reliability of the energy calibration, we show in Fig. 2 the α–α (top panel-left) and α–d (bottom panel-left) correlated spectra as a function of total kinetic energy in the center-of-mass of the two particles (CM), $E_{\mathrm{tot}} = \sum_i E_i^{(\mathrm{CM})}$, and, respectively, excitation energy ($E_{\mathrm{ex}} = E_{\mathrm{tot}} - Q$). For α–α correlation we considered the QP event sample described above. For α–d, we have additionally set the deuteron multiplicity to at least 1. The solid lines correspond to the peak fits using a Breit–Wigner distribution and peak centroids are pointed out by arrows. One may see that the α–α spectrum shows a narrow peak centered at 92 keV ($\Gamma = 84$ keV) and a much broader peak centered around 3 MeV. The first peak corresponds to the ground state of ^{8}Be ($Q = -92$ keV) with $\Gamma^{\mathrm{exp}} = 5.57$ eV and the second one to the first excited state at 3.03 MeV ($\Gamma^{\mathrm{exp}} = 1.5$ MeV). The α–d spectrum shows a well-formed peak centered at 2.23 MeV ($\Gamma = 570$ keV) corresponding to the first excited state of ^{6}Li at 2.186 MeV ($\Gamma^{\mathrm{exp}} = 24$ keV). In both cases, the low energy levels are accurately determined (within 40–50 keV), meaning that the charged particle energy calibration is trustworthy. At variance with this, information on higher excited levels is blurred by particles originating from other decays whose abundance increases with energy. Nevertheless, contamination of spectra may be removed to a large extent by employing correlation function techniques which account for how much the correlation within the physical event differs from the underlying single particle phase space.

Correlation functions (CF) are defined as the ratio between the correlated (physical) yield Y_{corr} and the product of single particle yields, generically termed as uncorrelated spectrum Y_{uncorr}, measured under the same conditions,

$$1 + R(X) = \frac{Y_{\mathrm{corr}}(X)}{Y_{\mathrm{uncorr}}(X)}. \tag{1}$$

Y_{uncorr} can also be built by mixing particles from different events as it is done in this work. In multi-particle CF [17], the generic variable X is represented by the total kinetic energy of the parti-

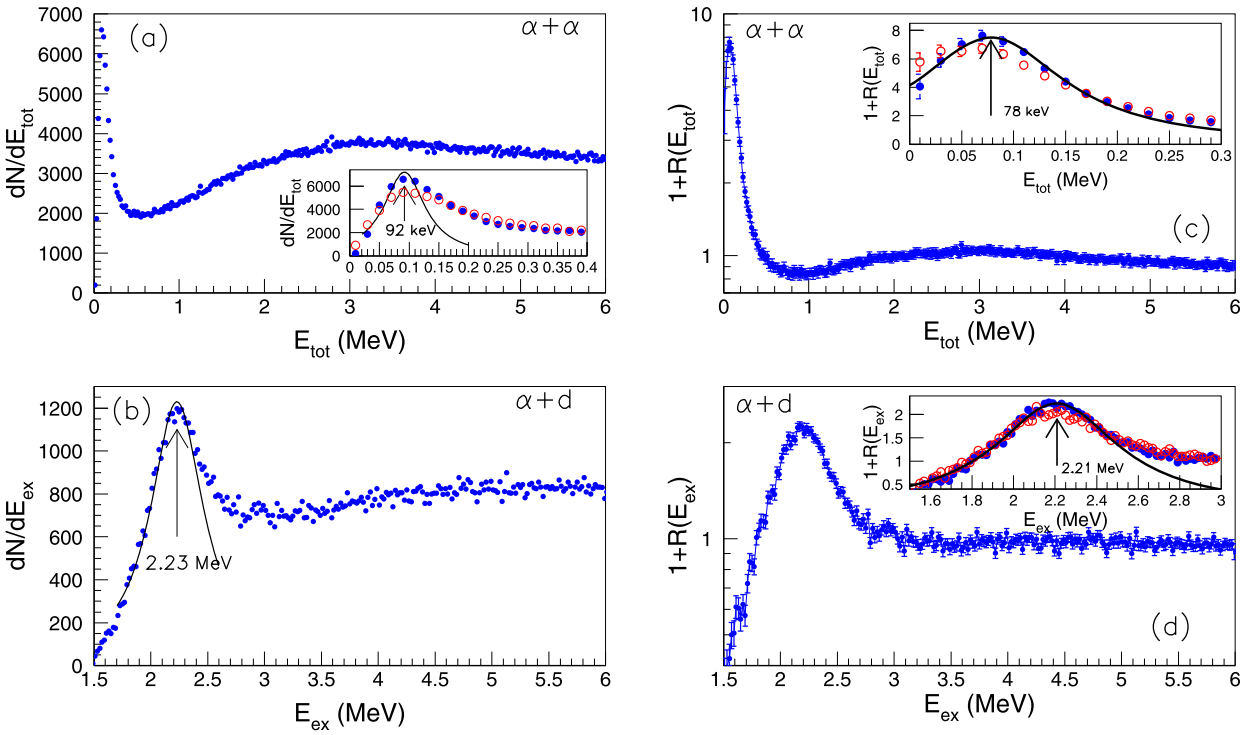

Fig. 2. (Color online.) Yields of correlated α–α (a) and α–d (b) emissions out of QP expressed as a function of total kinetic energy (a) or excitation energy (b) and corresponding correlation functions (c) and (d). The insets in (a) and (c) correspond to zooms on the ^{8}Be(g.s.) peak. The inset in (d) details the α–d correlation function in the domain of ^{7}Li(2.19 MeV). Peak fits using Breit–Wigner distributions are illustrated with solid lines, while centroids are pointed by arrows. Full and open symbols in the insets correspond to different ways of calculating the angle under which the detected particles were emitted (see text).

cles of interest in their center-of-mass frame $E_{\rm tot}$, by the excitation energy of their emitting source/state, $E_{\rm ex} = E_{\rm tot} - Q$ or, in the case of two-particle correlations, by the relative momentum. In nuclear physics, CF have been exploited to access spectroscopic properties [18], give space–time information taking advantage of proximity effects induced by Coulomb repulsion, and emphasize any production of events or sub-events with specific rare partitions [17,19,20]. The flat shape of the α–d CF around $1 + R(X) = 1$ at $E_{\rm ex} > 3$ MeV (see (d) of Fig. 2) confirms that the uncorrelated spectra are under control.

Both correlated spectra and CF manifest a peak broadening. This is a genuine consequence of detector finite granularity and energy resolution. Numerical simulations confirm that experimental distributions are compatible with an average energy resolution of detected α-particles R_E of 2%. The finite granularity is also responsible for a certain imprecision in the determination of the energy. To illustrate this, the insets in Fig. 2(a), (c) and (d) confront the correlated spectra and CF obtained under different hypotheses on the angle under which the detected particles were emitted. In the first case (solid symbols) we considered that all the particles which hit a certain module have been emitted under the angle corresponding to the geometrical center of that module. An alternative solution is to attribute to each particle a random angle in the domain allowed by the geometrical extension of the detector (open symbols). For all considered cases, the two scenarios lead to similar results, though the first hypothesis is preferable as producing smoother distributions and no extra broadening. In what follows only results obtained under the first hypothesis will be presented.

Information on the α-particle unstable excited states of ^{12}C populated by the ^{40}Ca + ^{12}C at 25 MeV/nucleon reaction may be extracted from the 3α-CF. The CF plotted in Fig. 3 correspond to the whole set of events with $m_\alpha = 3$ and an uncorrelated spectrum built by full event mixing (i.e. each particle belongs to a different physical event). The error bars are calculated consider-

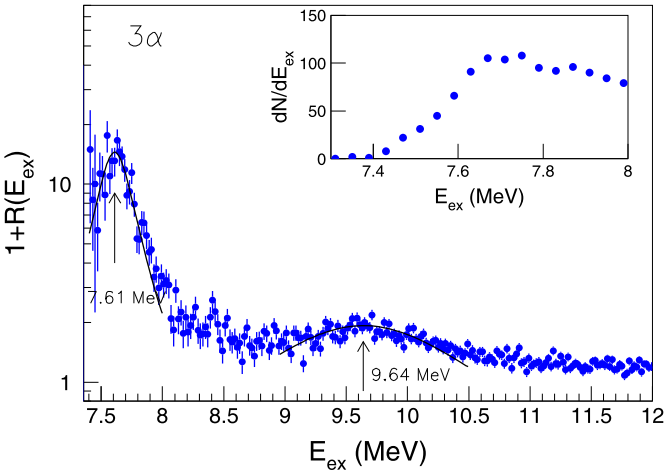

Fig. 3. (Color online.) 3α correlation function as a function of excitation energy. The arrows correspond to centroids of Breit–Wigner distributions (solid lines). Inset: zoom of the correlated spectrum in the energy domain of the Hoyle state.

ing only the statistical errors of the correlated spectrum. Errors on the uncorrelated spectra have been reduced to negligible values by increasing the number of uncorrelated events as compared to correlated events. The CF show two peaks centered at $E_{\rm ex} = 7.61$ MeV ($\Gamma = 0.33$ MeV) and $E_{\rm ex} = 9.64$ MeV ($\Gamma = 1.14$ MeV). The first peak corresponds to the Hoyle state ($E_{\rm ex}^{\rm exp} = 7.654$ MeV, $\Gamma^{\rm exp} = 8.5$ eV), while the second one is due to the complex region of excitations, characterized by the strong $E_{\rm ex}^{\rm exp} = 9.64$ MeV ($\Gamma^{\rm exp} = 34$ keV), 3^- state and by the broad $E_{\rm ex}^{\rm exp} = 10.3$ MeV, 0^+ state submerging a possible 2^+ state at 9.7 MeV [21,22]. As before, the peak centroids reproduce well the experimental excitation energy values, while a significant broadening comes from

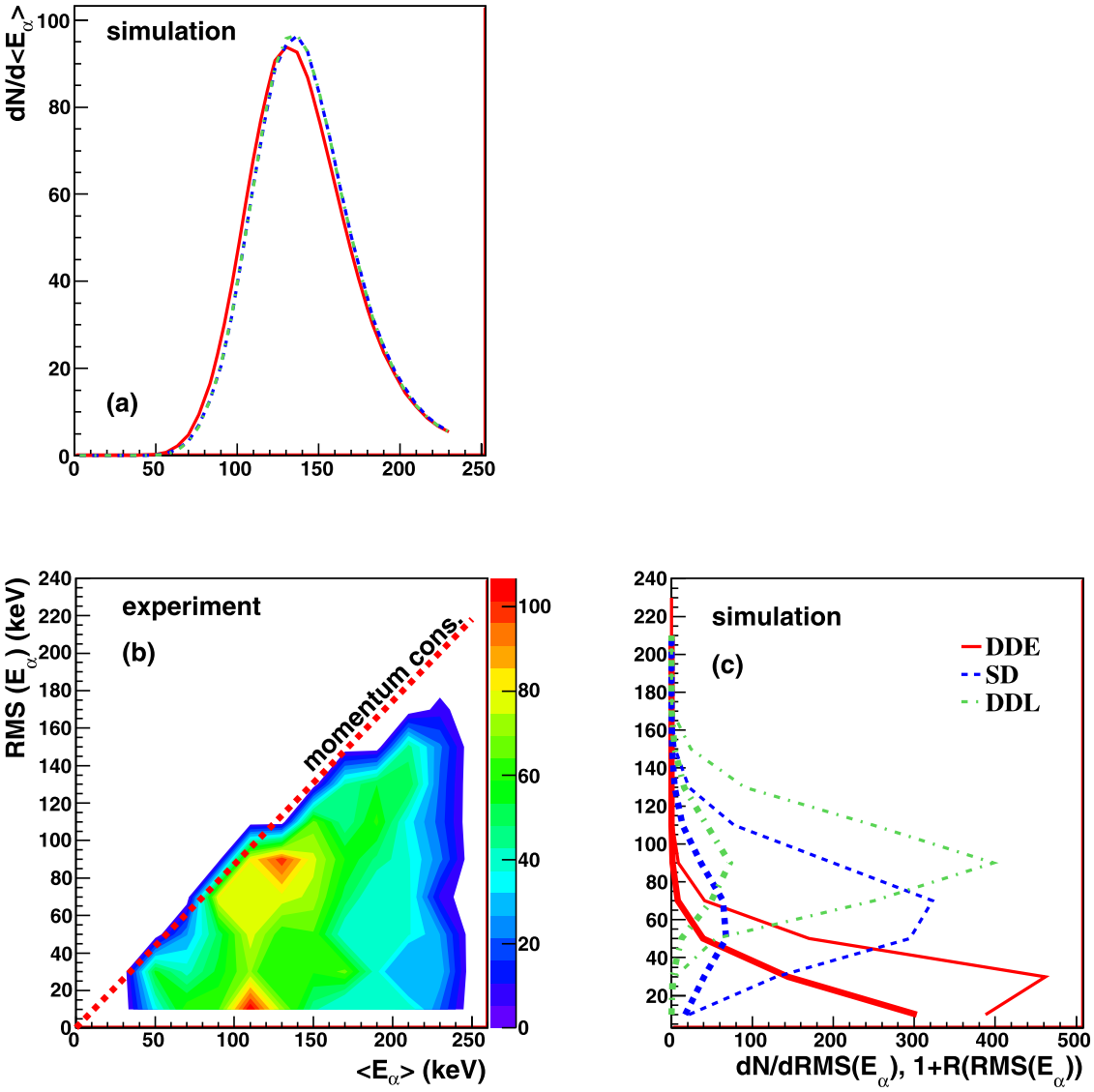

Fig. 4. (Color online.) Experimental 3α correlation function (b) expressed as a function of average kinetic energy – RMS of α-particles corresponding to 1072 experimental events with $7.37 \leqslant E_{ex} \leqslant 7.97$ MeV. The uncorrelated yield is built such as to allow for decay through ^{8}Be. The dotted line marks the maximum RMS compatible with momentum conservation. $\langle E_\alpha \rangle$ (a) and RMS (c) spectra (normalized to 1072 events) of simulated DDE (solid lines), SD (dashed lines) and DDL (dot-dashed lines) decays of the Hoyle state after filtering through the detector replica with $R_E = 2\%$. Panel (c) presents also the RMS projection of $Y_{\rm corr}(\langle E_\alpha \rangle, {\rm RMS})/Y_{\rm uncorr}(\langle E_\alpha \rangle, {\rm RMS})$ (thick lines).

the non-ideal detector properties (granularity and energy resolution). The inset of Fig. 3 illustrates the correlated spectrum in the energy domain of the Hoyle state and allows us to estimate the relative amount of genuine 3α decays versus background events. In the domain 7.37–7.97 MeV this ratio amounts to 1.

We demonstrated so far that the ^{40}Ca + ^{12}C nuclear reaction at 25 MeV/nucleon populates excited states of ^{12}C nuclei which decay by 3α emission. We now search for possible direct decays of the Hoyle state into equal energy particles (DDE) and, eventually, estimate their branching ratio. The existence of DDE is manifest when looking at the two-dimensional CF in the $\langle E_\alpha \rangle$-RMS plane (Fig. 4(b)); $\langle E_\alpha \rangle$ is the average kinetic energy of α-particles in their CM reference frame and ${\rm RMS} = \sqrt{\langle E_\alpha^2 \rangle - \langle E_\alpha \rangle^2}$. The uncorrelated spectrum is built by partial event mixing [23] of experimental events by taking two particles from the same event, in order to mimic for decay through ^{8}Be, while the third one stems from a different event. The peak of the correlation function localized at $\langle E_\alpha \rangle = 110$ keV and very low RMS $\leqq$ 25 keV corresponds to an equal sharing of the available energy of the Hoyle state among the three α-particles. Note that 110 keV corresponds to the value of the maximum of the CF of Fig. 3: 110 keV $\simeq (7610 + Q)/3$. To go further in the interpretation of the CF and estimate branching ratios, the experimental results were compared to numerical Monte–Carlo simulations filtered by the multi-detector replica. These are performed by considering ^{12}C nuclei excited in the Hoyle state and boosted with a velocity distribution identical to the experimental one. They decay by one of the following mechanisms: (1) direct emission in three α-particles with equal energies (DDE), (2) sequential decay proceeding via the g.s. of ^{8}Be with isotropic emission of the two α-particles from ^{8}Be (SD) and (3) direct α decay from a linear chain (DDL) [24,25] with an α at rest and an equal sharing of the available energy of the Hoyle state between the two other α-particles. Limitation of direct decays (DD), which in principle assume random energy sharing among the emitted particles, to the particular sub-class of DDE is due to the predicted condensate nature of the Hoyle state. In each case and, for sequential decay, at each decay step the available energy ($E_{ex} + Q$) is shared among the reaction products so as to conserve the linear and angular mo-

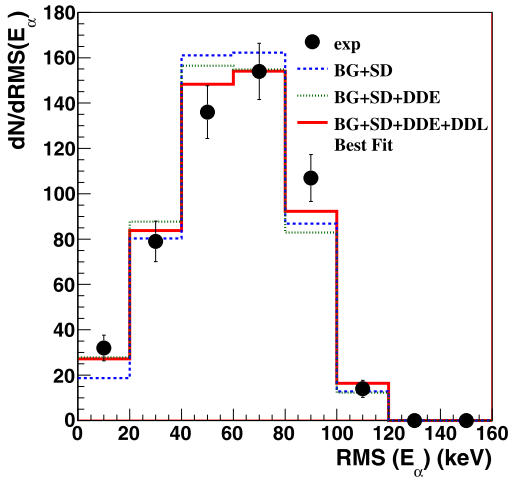

Fig. 5. (Color online.) RMS spectra of experimental (solid points) and best χ^2 simulated events (solid line) in the region $90 \leqslant \langle E_\alpha \rangle \leqslant 150$ keV. Experimental error bars are statistical. Dashed and dotted histograms illustrate simulation results if only sequential decay (60%) and, respectively, sequential decay (55.5%) + DDE (4.5%) are considered. In all cases, background (BG) events amount to 40%.

menta and, eventually, obey the postulated particularities of the decay. No preferential orientation between emitted particle velocities and source boost exists. The obtained reaction products are assumed to freely propagate toward the detector. Once the detector is reached, the events are filtered: if one or more particles hit a dead detector area or a detector which is out of work, the event is suppressed. If all particles have been detected, the velocity vectors are altered such as to account for finite angular and energy resolution. The simulated events are then analyzed as the experimental ones. The obtained detection efficiencies vary from 41 to 49% depending on the decay type. A comparison of filtered and normalized DDE (full), SD (dashed) and DDL (dot-dashed) simulations is depicted with thin lines in Fig. 4 as a function of $\langle E_\alpha \rangle$ (a) and RMS (c). Very little sensitivity on the decay mechanism of $Y_{\rm corr}(\langle E_\alpha \rangle)$ is observed, which is due to the angular resolution of the detection modules. By contrast, the kinetic energy dispersion (RMS) in the emitter CM manifests measurable sensitivity to the decay mechanism. For the CHIMERA granularity and a perfect energy resolution $Y_{\rm corr}$(RMS) are peaked at 10, 70 and 90 keV for DDE, SD and, respectively, DDL while for an average resolution $R_E = 2\%$ the corresponding values are 30, 70 and 90 keV. This suggests that searching for the best agreement between experimental and simulated $Y_{\rm corr}(\langle E_\alpha \rangle, {\rm RMS})$ constitutes a pertinent procedure to quantify each decay channel. Not surprisingly, the general category of DD with random energy sharing (not considered hereafter) leads to a broad $Y_{\rm corr}$(RMS) distribution which, under our experimental conditions, looks very similar to the dominating SD [12]. For a realistic reproduction of the experimental data, we add to the pure simulated events the same proportion of background events that exists in the data. These are produced by partial event mixing [23] of experimental events. The comparison is restricted to the energy domain, $7.4 \leqslant E_{\rm ex} \leqslant 7.8$ MeV, to reduce the importance of background events to 40%. Applying a χ^2 minimization procedure and correcting for efficiencies, we infer that $7.5 \pm 4.0\%$ of events correspond to DDE, $9.5 \pm 4.0\%$ to DDL and $83.0 \pm 5.0\%$ to SD. Error bars are estimated by taking into account statistical, χ^2 and background errors. The RMS(E_α) spectrum of simulated events (solid line) corresponding to the best χ^2 and the energy domain $90 \leqslant \langle E_\alpha \rangle \leqslant 150$ keV is displayed in Fig. 5 and compared to the corresponding experimental data (solid points). Note that a limitation to DDE and SD as possible decays (dotted histogram) leads to a significant increase of $\chi^2_{\rm min}$ without changing the DDE percentage. Results of simulations in which one allows only for SD are plotted with dashed lines for the sake of completeness. As one may notice, they correspond to a worse agreement with the data, particularly a sizeable underestimation of the number of low-RMS events. In all cases, the amount of background events is 40%.

Finally we can now fully understand the CF pattern (Fig. 4(b)); panel (c) of the figure presents also the simulated behaviors of $Y_{\rm corr}({\rm RMS})/Y_{\rm uncorr}({\rm RMS})$ (thick lines). Apart from DDE, the broad region around $\langle E_\alpha \rangle = 90$–$130$ keV and centered at RMS ≈ 70 keV corresponds to the sharing of the available energy between the two α's of ^{8}Be and the remaining α of 191 keV. The peak at $\langle E_\alpha \rangle \approx 130$ keV and RMS $= 90$ keV corresponds to the direct decay of a linear chain. Though the CF show, as expected, a certain sensitivity to the event selection or event mixing recipe, their overall pattern remains stable. Particularly the DDL peak of the CF is systematically shifted by about 20 keV with respect to the DDE one. As early mentioned, a small shift of the correlated spectrum is attributed to the finite size of detection modules (see Fig. 4(a)). An extra shift could be introduced by statistical effects.

A more popular way to visualize competing 3-particle decay mechanisms is the Dalitz plot. In this representation, DDE events must concentrate around the origin. Fig. 1 in reference [26] shows that our data manifest this pattern. Note also that, because of limited statistics and background, the rest of the figure cannot be interpreted.

The same analyses have been performed for the complex region centered at 9.64 MeV where the statistics is much higher; no indication in favor of a direct 3α decay with equal energies has been obtained [26]. For the 0^+_6 state at 15.097 MeV of ^{16}O the statistics is too poor to allow unambiguous interpretation of low RMS events.

In conclusion, the nuclear reaction ^{40}Ca + ^{12}C at 25 MeV/nucleon bombarding energy was used to produce states theoretically predicted as α-particle condensate states. Supposing that equal values of kinetic energy of the emitted α-particles represent a sufficient criterion for establishing the existence of α-particle condensation, we found that $7.5 \pm 4.0\%$ of events corresponding to the Hoyle state decay fulfill this criterion. To our knowledge, this is the first direct experimental indication of α-particle condensation in nuclei. This study also evidenced the presence of direct α decays from a linear α-chain as recently theoretically mentioned [24,25]. An experiment with higher statistics is planned to study the ^{16}O case.

Acknowledgements

The authors are indebted to P. Schuck for numerous discussions and one of the authors Ad.R.R. acknowledges the partial financial support from ANCS, Romania, under grant Idei No. 267/2007.

References

[1] L.P. Pitaevski, S. Stringari, Bose–Einstein Condensation, Clarendon Press, Oxford, 2003.
[2] G. Röpke, A. Schnell, P. Schuck, P. Nozieres, Phys. Rev. Lett. 80 (1998) 3177.
[3] M. Beyer, S.A. Sofianos, C. Kuhrts, G. Röpke, P. Schuck, Phys. Lett. B 448 (2000) 247.
[4] T. Sogo, R. Lazauskas, G. Röpke, P. Schuck, Phys. Rev. C 79 (2009) 051301.
[5] A. Tohsaki, H. Horiuchi, P. Schuck, G. Röpke, Phys. Rev. Lett. 87 (2001) 192501.
[6] Y. Funaki, T. Yamada, H. Horiuchi, G. Röpke, P. Schuck, A. Tohsaki, Phys. Rev. Lett. 101 (2008) 082502.
[7] M. Chernykh, H. Feldmeier, T. Neff, P. von Neumann-Cosel, A. Richter, Phys. Rev. Lett. 98 (2007) 032501.
[8] E. Uegaki, Y. Abe, S. Okabe, H. Tanaka, Prog. Theor. Phys. 57 (1977) 1262.
[9] S. Ohkubo, Y. Hirabayashi, Phys. Rev. C 70 (2004) 041602(R).
[10] T. Yamada, P. Schuck, Phys. Rev. C 69 (2004) 024309.
[11] W. von Oertzen, Eur. Phys. J. A 29 (2006) 133.
[12] M. Freer, et al., Phys. Rev. C 49 (1994) R1751.

[13] F. Hoyle, et al., Phys. Rev. 92 (1953) 1095.
[14] C.W. Cook, et al., Phys. Rev. 107 (1957) 508.
[15] A. Pagano, et al., Nucl. Phys. A 734 (2004) 504.
[16] L. Morelli, et al., Nucl. Instr. Meth. A 620 (2010) 305.
[17] R.J. Charity, et al., Phys. Rev. C 52 (1995) 3126.
[18] W.P. Tan, et al., Phys. Rev. C 69 (2004) 061304.
[19] Y.D. Kim, et al., Phys. Rev. C 45 (1992) 338.
[20] G. Tabacaru, et al., Eur. Phys. J. A 18 (2003) 103.
[21] M. Itoh, et al., Nucl. Phys. A 738 (2004) 268.
[22] M. Freer, et al., Nucl. Phys. A 834 (2010) 621c.
[23] F. Grenier, et al., Nucl. Phys. A 811 (2008) 233.
[24] H. Matsumura, Y. Suzuki, Nucl. Phys. A 739 (2004) 238.
[25] E. Epelbaum, et al., Phys. Rev. Lett. 106 (2011) 192501.
[26] Ad.R. Raduta, et al., Int. J. Mod. Phys. E 20 (2011) 902.